Equal-strength Beam Design of Acoustic Wave Accelerometers

Authors

Yihan Zhao[1], Jian Zhou[1,], Linjuan Kuang[1], Yihao Guo[1], JianFei Xie[1], Yongqing Fu[2]*

Affiliations

1. College of Mechanical and Vehicle Engineering, Hunan University, Changsha 410082, China
2. Nursing Department, Third Xiangya Hospital, Central South University, Changsha, 410013, China.
3. Faculty of Engineering and Environment, Northumbria University, Newcastle upon Tyne, NE1 8ST, United Kingdom

* Corresponding author E-mail: jianzhou@hnu.edu.cn

Abstract: Surface acoustic wave (SAW) based accelerometers have received significant attention due to their digital output, low cost, mass production and easy implementation of wireless passive function. However, conventionally rectangular cantilever-beam based SAW accelerometers often have non-uniform strains generated along the beams, which cause emergence of parasitic wave modes and measurement errors. In this paper, a simulation platform was developed to analyze and optimize designs of SAW accelerometers and variable-thickness and equal-strength beams were designed to solve the critical issue of non-uniform strain distribution along the beam. Frequency responses of SAW accelerometers under the acceleration were successfully obtained using the simulation platform, with the visualized strain/stress distribution and particle displacement field. The accuracy of this simulation platform was verified using the experimental result reported in literature. A highly sensitive and equal-strength beam SAW accelerometer was achieved with a sensitivity up to 1.40 kHz/g, a linearity coefficient of ~1, and a measurement range of 0~15 g. Furthermore, a high-G accelerometer was designed, with the capability of enduring large shocks up to 11,500 g and a sensitivity of 6.96 Hz/g.

Keywords: SAW, accelerometer, simulation, equal-strength beam, high-G

1. Introduction

Micro-electro-mechanical system (MEMS) based accelerometers have experienced tremendous development over the last decade, with significantly increasing applications for automotive safety, rail transit, aerospace field and smartphones[1-4]. Compared with the conventional accelerometers, MEMS based accelerometers possess many advantages such as small size, light weight, low cost, low power consumption, and ease of integration with semiconductor technology[5]. Capacitive accelerometers[6], piezoresistive accelerometers[7], resonant accelerometers[8], tunneling accelerometers[9] and surface acoustic wave (SAW) accelerometers are the most commonly reported MEMS accelerometers. Of these, SAW accelerometers, which is based on the principle that its resonant frequency is shifted caused by changes in parameters such as elastic constants and densities of the piezoelectric material under the acceleration, have received significant attention due to their digital output, mass production capacity and easy implementation of wireless passive detection[10].

A typical SAW accelerometer is made of a cantilever beam with one end fixed and the other being free, while the SAW device is integrated onto the surface of the cantilever near the fixed end where stress or sensitivity is the highest. In 2014, Wang et al. proposed a wireless and temperature-compensated SAW vibration sensor utilizing Y-cut quartz cantilever beam[11]. In 2015, they further developed a SAW acceleration sensor incorporating ST-X quartz cantilever beam, achieving a high sensitivity up to 29.7 kHz/g, with a good linearity and a high resolution[12]. In 2015, Lukyanov et al. and designed the console of SAW accelerometer, making it able to survive extreme impact (50 g ~ 65,000 g) with a sensitivity of 0.2 Hz/g[13]. In 2020, Shevchenko et al. proposed a novel sensitive element using aluminum nitride membrane for acceleration measurement, and achieved a sensitivity of 43 Hz/g[14]. In 2022, the optimization strategy was further proposed by them to narrow the bandwidth and improve signal detection[15].

Despite notable advances in SAW accelerometer, it is worth noting that there often exist non-uniform strains along the beams, which may cause the emergence of a parasitic mode and a lot of measurement errors[16] for the conventional SAW accelerometers. To be specific, when a rectangular cantilever-beam based SAW accelerometer is subjected to a stress, the strain at the fixed end is the largest, and it will decrease to almost zero at the free end. To ensure that

the strain variation is small enough to minimize the measurement error, the cantilever beam should be long enough compared with the size of the SAW device. However, this will certainly increase the overall size of the accelerometer, which may cause limitation in application scenarios. To solve this problem, a variable-width triangular cantilever beam was previously proposed, providing uniform bending stresses at the length direction and achieving a sensitivity of 22.5 kHz/g within a measurement range -4~4 g[17]. Although the length of the cantilever beam in this design has been shortened significantly, the size at the width direction is inevitably increased. Another commonly used method is a ring-shaped sensitive element design for SAW accelerometer using the circular interdigital transducers (IDTs) [18, 19]. However, the aperture of SAW IDTs should be small enough, which restricts the high performance of SAW resonators.

Sensitivity is a crucial index of the performance of SAW accelerometers. Thus, it is important to obtain the theoretical value of frequency shift during design stage. Wang et al. calculated the theoretical value of the frequency shift by deriving the relationship between the frequency and the strain[11, 12], while a series of simplifications and approximations were involved in this process, which inadequately coupling the perturbation effect into the frequency shift. Lukyanov D. et al. directly multiplied the simulating strain on the beam surface and the initial resonant frequency to obtain the frequency shift[20], which lacked theoretical derivation and did not verify the accuracy of model. Ji et al. used mathematical iteration method by MATLAB to obtain the wave velocity under perturbation according to the relationship between the resonant frequency and the wave velocity[21]. This method basically takes into account the main effects caused by the perturbation and is more accurate, while the implementation is quite complicated for the requirement of in-depth knowledge of Mathematics and Physics. In addition, it was unable to provide sufficient visualization.

To overcome the above limitations, in this paper, we proposed an efficient and accurate simulation platform for design and optimization of SAW accelerometers utilizing COMSOL Multiphysics software based on finite element method (FEM). This platform can effectively simulate the frequency responses of SAW devices under the acceleration, visualize the distribution of strain/stress and particle displacement field of the sensor, and greatly simplify post-simulation for the related parameters. Meanwhile, the frequency shift could be displayed by the S-parameters with a parametric scan of acceleration. The accuracy of the model and

simulation platform was verified by the experiment results reported in Ref.[22]. With the help of this simulation platform, we proposed a variable-thickness equal-strength cantilever beam (**Figs. 1b&d**) to solve the issue of non-uniform strain distribution along the conventional cantilever. A high sensitivity of 1.40 kHz/g was obtained for such cantilever structure, with the measurement range of 0~15 g. Furthermore, a high-G accelerometer based on the equal-strength beam was also designed, as shown in **Figs. 1c&e**, with the capability of enduring large shocks of up to 11,500 g and a sensitivity of 6.96 Hz/g.

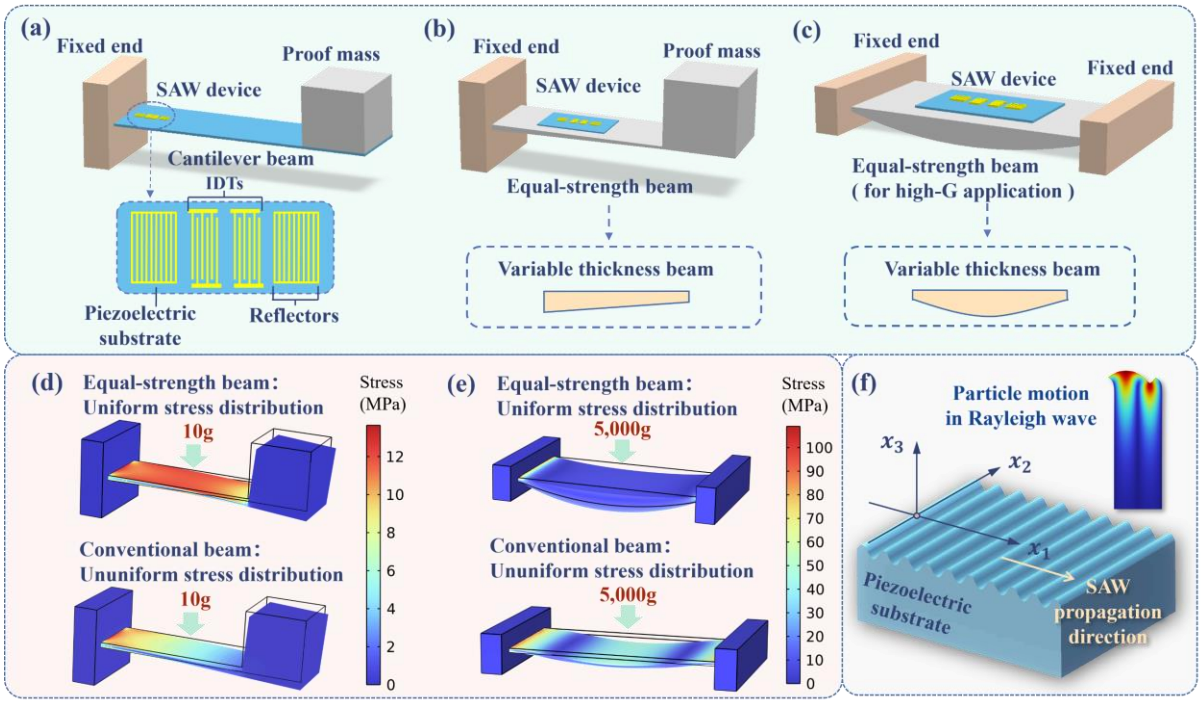

Figure 1. (a) The schematics of the tradition SAW accelerometer based on a cantilever beam and the two-port SAW resonator; (b) The schematic of accelerometer based on an equal-strength cantilever beam (variable thickness); (c) The schematic of accelerometer based on an equal-strength beam with double ends fixed (variable thickness) for high-G application; (d) The stress cloud diagram of equal-strength cantilever beam and conventional rectangular cantilever beam under acceleration of 10 g; (e) The stress cloud diagram of equal-strength beam and conventional rectangular beam under acceleration of 5,000 g; (f) Propagation of surface acoustic wave on elastic body in semi-infinite space and the particle's vibration displacement of SAW.

2. Theoretical Background and Verification of Simulation Platform

In order to avoid waste of resources, it is necessary to optimize the design of the devices

and evaluate their performance using simulation tools prior to devices fabrication. When a SAW accelerometer is subject to the acceleration, the acoustic velocity in piezoelectric elastic material changes as the strain is generated on the substrate according to perturbation theory, which appears as a shift of the resonant frequency. Therefore, it is necessary to study the wave equations in piezoelectric elastic material when it is unperturbed and perturbed respectively.

In piezoelectric medium, the excitation of SAW is based on piezoelectric effect, and the physical mechanism can be represented by piezoelectric constitutive equation:

$$\begin{cases} T_{ij} = c_{ijkl}S_{kl} - e_{kij}E_k \\ D_i = e_{ikl}S_{kl} + \varepsilon_{ik}E_k \end{cases} \quad (i,j,k,l = 1,2,3) \tag{1}$$

where The T_{ij} is the stress, c_{ijk} is the elastic constant, e_{kij} is the piezoelectric constant, ε_{ik} is the dielectric constant, D_i is the electric displacement, E_k is the electric field, S_{kl} is the strain. And

$$S_{kl} = \frac{1}{2}\left(\frac{\partial u_k}{\partial l} + \frac{\partial u_l}{\partial k}\right) \tag{2}$$

$$E_k = -\frac{\partial \phi}{\partial x_k} \tag{3}$$

where x_1 is the direction of the SAW's propagation and x_3 is normal to the substrate surface, as shown in **Fig. 1f**, u is the mechanical displacement of substrate surface, and Φ is the electric potential.

The interaction of mechanics and electricity leads to the coupling of acoustic wave and electromagnetic wave. In this case, the coupled wave equation is

$$\begin{cases} \dfrac{\partial T_{ij}}{\partial x_i} = \rho \dfrac{\partial^2 u_j}{\partial t^2} \\ D_{i,i} = 0 \end{cases} \tag{4}$$

where ρ is the density of piezoelectric substrate.

Substituting Eqs. (1) ~ (3) into Eq. (4), the wave equation of piezoelectric elastic material without perturbation can be obtained:

$$\begin{cases} c_{ijkl}\dfrac{\partial^2 u_k}{\partial x_i \partial x_l} + e_{kij}\dfrac{\partial^2 \phi}{\partial x_i \partial x_k} = \rho \dfrac{\partial^2 u_j}{\partial t^2} \\ e_{kij}\dfrac{\partial^2 u_k}{\partial x_i \partial x_l} - \varepsilon_{ik}\dfrac{\partial^2 \phi}{\partial x_i \partial x_k} = 0 \end{cases} \tag{5}$$

When the piezoelectric elastic material is subject to stress caused by the applied acceleration, the propagation of SAW will be affected as the piezoelectric substrate bends. By

incorporating the initial stress directly into the wave equation, Eq. (4) becomes[23]

$$\begin{cases} \dfrac{\partial T_{ij}}{\partial x_i} + \dfrac{\partial}{\partial x_i}\left(\sigma_{ik}\dfrac{\partial u_j}{\partial x_k}\right) = \rho\dfrac{\partial^2 u_j}{\partial t^2} \\ D_{i,i} = 0 \end{cases} \quad (i,j,k = 1,2,3) \tag{6}$$

where σ_{ik} denotes the initial stress.

Meanwhile, the initial stress also has influence on the elastic constants and density of the piezoelectric elastic material, because it is inhomogeneous in the case of bending deformation[24].

$$c'_{ijpq} = \mathrm{c}_{ijpq} + \mathrm{c}_{ijpqmn}\eta_{kl}, \qquad i,j,p,q,m,n = 1,2,3,4,5,6 \tag{7}$$

$$\frac{\Delta\rho}{\rho} \approx -(\mathrm{S}_1 + \mathrm{S}_2 + \mathrm{S}_3) \tag{8}$$

where c_{ijpq}, c_{ijpqmn} are the second-order and third-order elastic constants of the material without perturbation respectively, c'_{ijpq} is the second-order elastic constant under the perturbation, η_{kl} is the Lagrangian strain. And $\Delta\rho$ is the variation of the density.

By substituting Eqs. (1), (7) and (8) into Eq. (6), we can obtain the wave equation of piezoelectric elastic material under perturbation:

$$\begin{cases} \sigma_{ik}\dfrac{\partial^2 u_j}{\partial x_i \partial x_k} + c'_{ijkl}\dfrac{\partial^2 u_k}{\partial x_i \partial x_l} + e_{kij}\dfrac{\partial^2 \phi}{\partial x_i \partial x_k} = \rho'\dfrac{\partial^2 u_j}{\partial t^2} \\ e_{kij}\dfrac{\partial^2 u_k}{\partial x_i \partial x_l} - \varepsilon_{ik}\dfrac{\partial^2 \phi}{\partial x_i \partial x_k} = 0 \end{cases} \tag{9}$$

Consequently, the velocity and resonant frequency of SAW in piezoelectric elastic material under the perturbation of acceleration can be obtained by solving Eq. (9). Although Eq. (5) can be directly solved in the piezoelectric physics field provide by COMSOL when the acceleration is 0g[25], additional physics field and modifications are required because Eq. (9) is highly nonlinear. Detailed simulation setup based on this theoretical model in COMSOL is provided in supporting information (SI).

To verify the accuracy of the simulation platform, the simulation model was performed using the structure parameters reported in Ref. [22], as shown in **Fig. 2a**. Simulation parameters of the SAW resonator are listed in **Table 1**, and the wave type is Rayleigh wave, as shown in **Fig. 1f**. The obtained stress distributions and the displacements of the center lines of cantilever beam are shown in **Figs. 2b&c**. The frequency responses (i.e., the transmission coefficient S_{21})

of the SAW device under various accelerations are illustrated in **Fig. 2d**. Results show that the simulation model can visualize the particle displacements, stresses and frequency responses of the SAW accelerometer. In addition, the frequency of SAW device was linearly decreased with the increase of acceleration. The sensitivity of the accelerometer can be calculated using $S = \Delta f / a$, where S is sensitivity, Δf is the frequency shift, and a is the acceleration. It can be seen from the results that the simulating resonant frequency of 304 MHz has an error of 1.3%. And the simulating sensitivity of the SAW accelerometer is 26.87 kHz/g, which agrees well with the experimental value of 27 kHz/g reported in Ref. [22] with the error of 0.48%. **Fig. 2e** demonstrates the accuracy of our simulation platform by comparing the obtained sensitivity with that in Ref. [22] (the calculating value is ~34.5 kHz/g), where the black represents the frequency shift obtained by the simulation model proposed in this paper, the red represents the experimental results in Ref. [22] and the blue represents the theoretical results in Ref. [22].

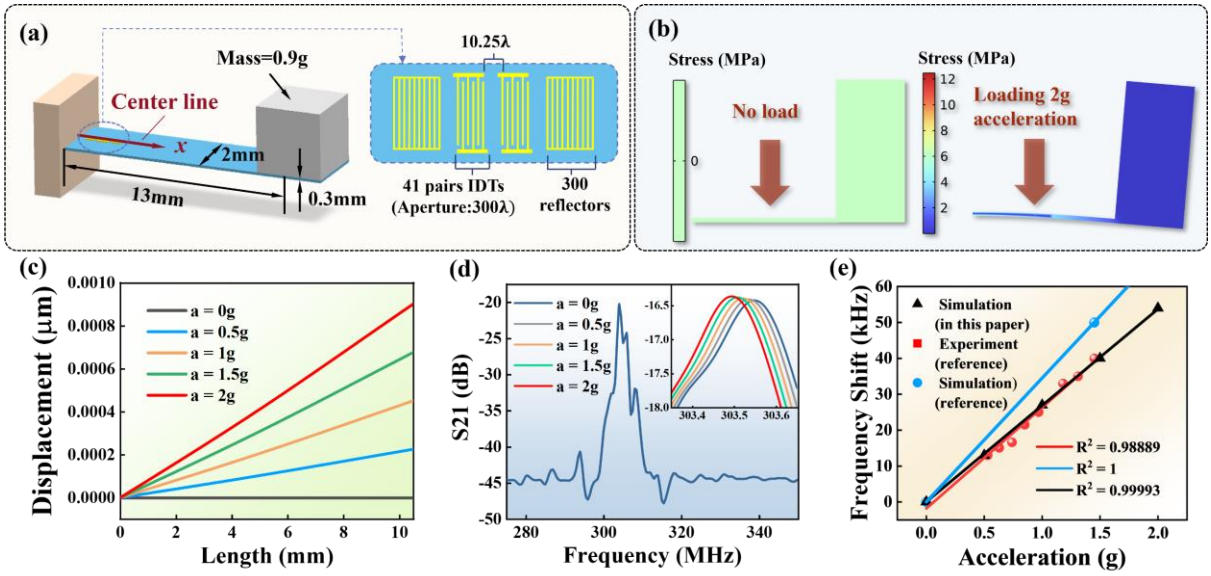

Figure 2. (a) The schematic of the SAW accelerometer in Ref.[22]; (b) Stress cloud diagram of surface acoustic wave accelerometer under no load and acceleration of 2g; (c) Displacement distribution along the center line of the cantilever beam; (d) The frequency response (transmission coefficient S21) of the SAW accelerometer with a range of 0~2g; (e) The sensitivity analysis and comparison between simulation results and experimental results.

Table 1. Simulation parameters of the SAW resonator.

Parameters	Value
Wavelength / λ (μm)	10.53
Width of electrode (μm)	2.63
Aperture	300λ
Electrode thickness (μm)	0.15
IDT pairs	41
Reflector pairs	300
Distance between IDT and reflector	0.25λ
Distance between IDTs	10.25λ

3. Theoretical Background and Design of Equal-strength Beam

The equal-strength beam structure design was proposed in this study to eliminate the effect of uniformly distributed strain along the beam. Specifically, the variable-thickness beam was designed, thus the axial dimension would be greatly reduced without any increase of the width of the beam, enabling the small plane-geometric dimensions. According to Hooke's Law, uniformly distributed strain means that the stress on the beam distributes uniformly when the SAW accelerometer is under acceleration.

Ideally, when a beam is subjected to pure bending, the normal stress at any point of the cross section is proportional to its distance away from the neutral axis, as shown in **Fig. 3a**. The surface of the beam where the SAW device is mounted is the farthest away from the neutral axis, so the stress on the beam surface is the largest. The relationship between the maximum normal stress and bending moment can be described as

$$\sigma_{max} = \frac{M}{W} \tag{10}$$

where σ_{max} indicates the maximum normal stress, M is the bending moment, and W is the section modulus in bending. Since the beam used in our design is rectangular and has variable thicknesses (**Fig. 3b**), the section modulus in bending is related to thickness:

$$W = \frac{1}{6} b h^2(z) \tag{11}$$

where *b* is the width of the cantilever beam, and *h(z)* is the thickness of beam at a certain cross section[26].

It is obvious that the magnitude of stress on the beam surface is related to the thickness of the beam, which means that the stress will change with the change of the beam thickness when the external force and the beam width are constant. In addition, the maximum normal stress should be smaller than the allowable stress $[\sigma]$,

$$\sigma_{max} \leq [\sigma] \tag{12}$$

Therefore, to achieve the equal-strength beam design (or the uniform distribution of stress/strain) and the maximum measurement range (or the maximum surface stress of beam), we can assume that the maximum stress is a constant, and the thickness of the beam *h(x)* can be obtained by substituting Eqs. (12) and (13) into Eq. (14)

$$h(x) = \sqrt{\frac{6M}{b[\sigma]}} \tag{13}$$

From the above equation, it can be seen that we only need to figure out the distribution of bending moment *M* on the surface of the beam in order to obtain the thickness of the beam that can ultimately achieve uniform stress distribution.

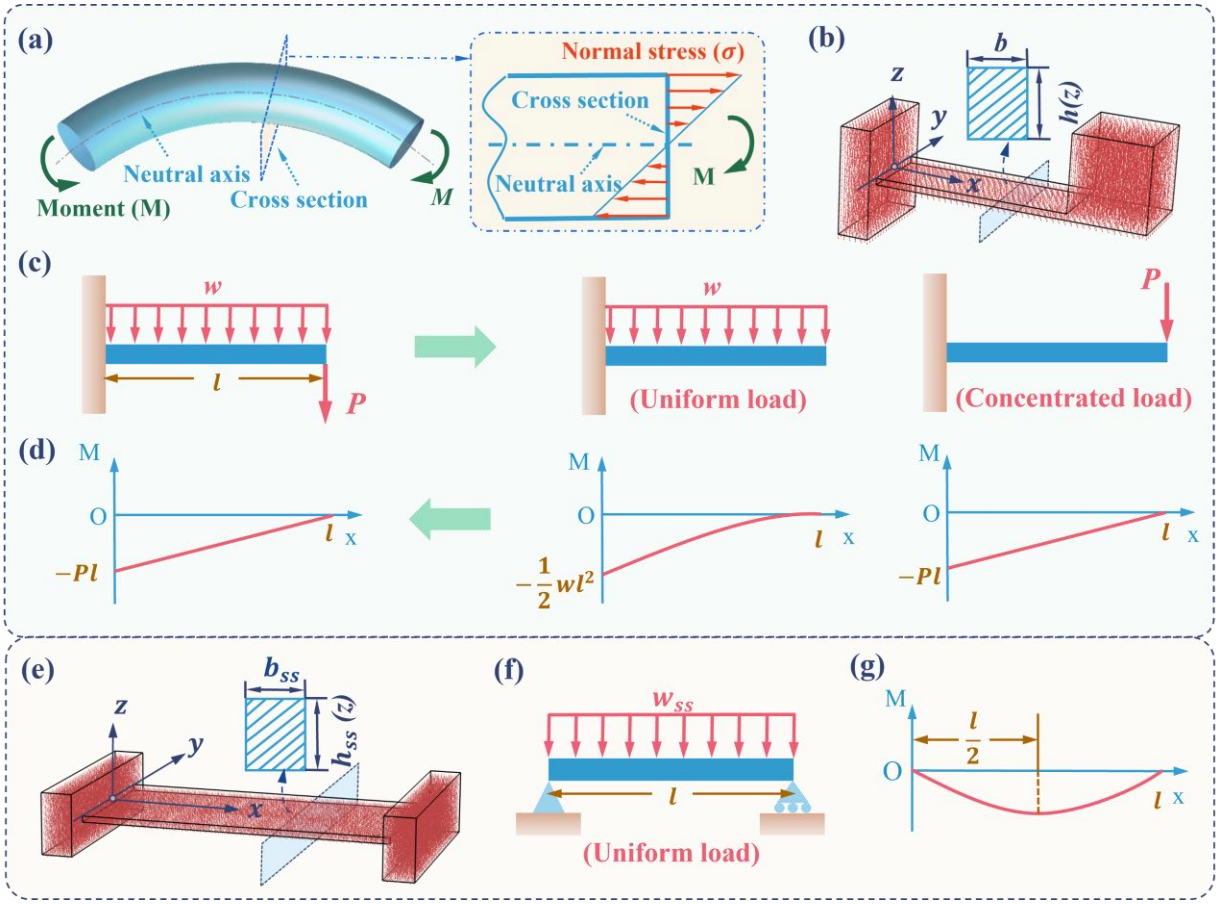

Figure 3. (a) A beam subjected to pure bending and the stress distribution of its cross section; (b) Load distribution of cantilever beam under acceleration load; (c) The force condition decomposition diagrams of cantilever beam under acceleration load; (d) The bending moment diagrams of the cantilever beam under different component forces; (e) Load distribution of the beam with two fixed ends under acceleration load; (f) The force condition analysis of the beam with two fixed ends under acceleration load; (g) The bending moment diagram of the beam with two fixed ends under uniform load.

3.1 Equal-strength Cantilever Beam Design

Before obtaining the bending moment *M*, it is necessary to analyze the force condition of the beam. When a cantilever beam is accelerated, the applied force is a combination of a concentrated load *P* (induced by the proof mass) and a uniformly distributed load with a load collection degree *w* (induced by the beam itself) according to the superposition principle, as shown in **Fig. 3c**. The cross-section method is employed during the analysis below, which is a general method to obtain internal forces in the mechanics of materials.

Taking the length direction of the beam as the x-axis, the internal shear force $F_1(x)$ of the

cross section and bending moment $M_1(x)$ of the cross section under the uniform load (w) can be written using:

$$F_1(x) = w(l - x), \qquad 0 < x < l \tag{14}$$

$$M_1(x) = \frac{1}{2}w(l - x)^2, \qquad 0 \le x \le l \tag{15}$$

where, l is the length of the beam.

In addition, the internal shear force $F_2(x)$ of the cross section and bending moment $M_2(x)$ of the cross section under the concentrated load P are:

$$F_2(x) = P, \qquad 0 < x < l \tag{16}$$

$$M_2(x) = -P(l - x), \qquad 0 \le x \le l \tag{17}$$

Therefore, the whole bending moment of cross section (**Fig. 3d**) is the sum of the bending moment induced by uniform load w and that by concentrated load P, i.e., $M_1(x) + M_2(x)$.

It should be noted that, effect of the concentrated load P is much larger than the uniform load w, especially when the beam is very thin and the mass of the proof mass is large. Therefore, the whole bending moment of cross section $M(x)$ is approximately equal to the $M_2(x)$ (**Fig. 3d**),

$$M(x) = M_1(x) + M_2(x) \approx M_2(x) = -P(l - x) \tag{18}$$

By substituting the Eq. (20) into Eq. (15), the thickness of cantilever beam can be obtained as:

$$h(x) = \sqrt{\frac{6|-P|(l - x)}{b[\sigma]}} \tag{19}$$

The above analysis indicates that if the thickness of beam exactly satisfies the theoretical equations, a perfect equal-strength beam can be achieved ideally. Unfortunately, the bending moment changes with the change of acceleration, which means the thickness of the beam is different under different accelerations as well. Therefore, it is difficult to achieve the equal strength for every case practically. Further simplification is necessary to optimize the thickness of the beams for accelerometers by simulation.

From the above equation, we can observe that, for equal-strength cantilever beam design, the thickness of cantilever beam is gradually decreased from the fixed end to the free end. When the X =0 (at the point of fixed end of beam), the thickness of cantilever beam has the largest value, and the thickness has the smallest value when the X=l.

Considering the short length of the cantilever beam, we simplified the thickness curve to a linear one, that is, the thickness of its fixed end was proportional to the thickness of its free end. The ratio of two ends' thickness of cantilever beam was set as a variable (as shown in **Fig. 4a**), and the optimal ratio was systematically investigated. According to Eq. (19), the thickness of single ended cantilever beam should be converged to zero at the free end, which is impracticable in practice. The thickness of the free end in our work was set to be 0.2 mm here(the value is consistent with the previous experimental structure parameters[22]). The beam length was set as short as possible to just fit the requirement of mounting SAW device. The proof mass was 13 times as much as that of the cantilever beam. The structure parameters of design are summarized in **Table 2**.

Fig. 4b shows the effect of the thickness ratio (ranging from 1 to 3) on the stress distribution of cantilever beam surface. Results show that when the ratio is 1 (which means the conventional rectangular beam), the cantilever beam has an uneven stress distribution. With the ratio increased from 1 to 1.8, the stress distribution becomes more uniform. Whereas it becomes uneven again when the ratio is further increased from 1.8 to 3. Accordingly, the optimized thickness ratio between the two ends of cantilever beam is 1.8.

Table 2. The structure parameters of equal-strength beams design.

Parameters	**Symbols/values of equal-strength cantilever beam**	**Symbols/values of equal-strength simply supported beam**
Beam length (mm)	L = 10	L_{ss} = 10
Beam width (mm)	b = 5	b_{ss} = 5
Constant beam thickness (mm)	h_1 = 0.2	h_{ss_2} = 0.2
Variable beam thickness (mm)	h_2	h_{ss_1}
Thickness ratio	h_2/h_1	h_{ss_1}/h_{ss_2}
Proof mass and beam mass ratio	13	/

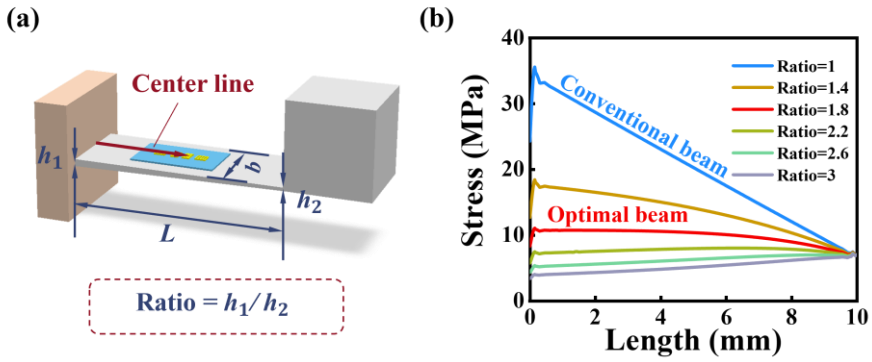

Figure 4. (a) The geometrical dimension of the SAW accelerometer based on an equal-strength cantilever beam; (b) Stress distribution along center line of different thickness ratio of the cantilever beam.

3.2 Equal-strength Beam for High-G Design

A simply supported beam with double-ended fixed (**Fig. 3e**) was proposed to withstand high acceleration shock for SAW accelerometer. The design principle is similar to that of single ended cantilever beam. However, for the double-ended fixed beam, there is only a uniformly distributed load with a load collection degree w_{ss}, as shown in **Fig. 3f**. In this case, the whole bending moment of cross section $M_{ss}(x)$ **(Fig. 3g)** can be described using the following equation,

$$M_{ss}(x) = \frac{1}{2} w_{ss} l x - \frac{1}{2} w_{ss} x^2, \qquad 0 \le x \le l, \tag{20}$$

By substituting this equation into Eq. (15), the thickness of equal-strength beam for high-G is obtained as:

$$h_{ss}(x) = \sqrt{\frac{6\left|\frac{1}{2} w_{ss} l x - \frac{1}{2} w_{ss} x^2\right|}{b_{ss}[\sigma]}} \tag{21}$$

From the above formula, it can be seen that this equal-strength beam has the feature of being thick in the middle and thin at both ends.

Fig. 5a shows the designed structure of an equal-strength beam for high-G SAW accelerometer according to Eq. (21). This is also often called 'fish-belly beam' and widely used in the construction of bridges and house beams. We set the ratio of two ends' thickness of the beam as a variable, and carried out a parametric scan of it. Similar to the cantilever beam, the stress distribution becomes uniform and then ununiform again as the ratio increases. **Fig. 5b** presents effects of the thickness ratio on the stress distribution, indicating that the optimized

ratio is 5.

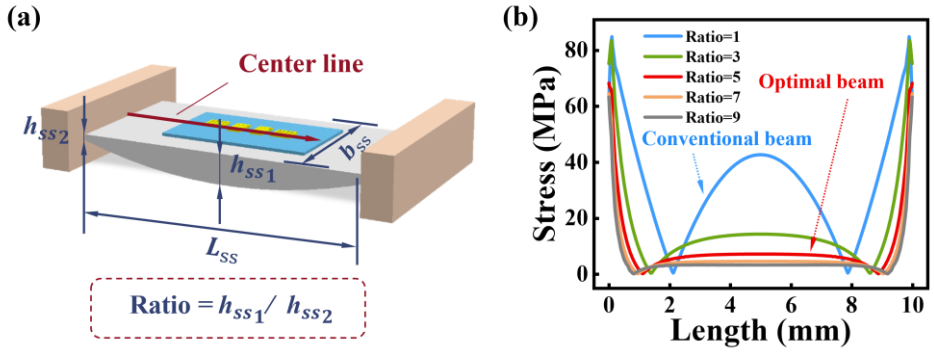

Figure 5. (a) The geometrical dimension of the SAW accelerometer based on an equal-strength simply supported beam; (b) Stress distribution along center line of different thickness ratio of the simply supported beam.

4. Simulation Results and Discussion

4.1 SAW Accelerometers Integrated with Equal-strength Cantilever Beam

Simulations of equal-strength beams were carried out on the basis of the optimization mentioned above. We additionally simulated a set of SAW accelerometers with rectangular beams and controlled the variables of these structures (materials, length and width of beams, weight of proof mass and applied acceleration) for a powerful and clear comparison.

The area with uniform stress distribution of the variable thickness beam is clearly larger than that of the rectangular beam, as shown in **Figs. 6a**, which demonstrates that the proposed design of equal-strength cantilever beam works well. The stress distribution curve along center line of conventional rectangular cantilever beam is much steeper than that of equal-strength cantilever beam, as shown in **Fig. 6b**. Therefore, the proposed equal-strength cantilever beam is robust to the mounting error of SAW device at the length direction where the SAW device can collect similar strain. According to **Fig. 6c**, the measuring range should be within 15 g.

The performance of the accelerometer integrated with proposed cantilever beam was investigated using the simulation model in Section 2. The beam and the proof mass are metal(Q235) and the material parameters[27, 28] are listed in SI. The simulation parameters of the SAW resonator are listed in **Table 1** but with 7x5x0.5mm ST-quartz as the substrate, and the SAW device also works in Rayleigh wave mode. Parametric scan of acceleration is carried

out to display the frequency shifts intuitively, and **Fig. 6d** illustrates the obtained frequency shifts of the designed equal-strength cantilever beam of SAW accelerometer under the acceleration from 0~15g. Results shows that the frequency shift has a good linear relationship with a perfect linearity and a predicted sensitivity of 1.4 kHz/g (**Fig. 6e**).

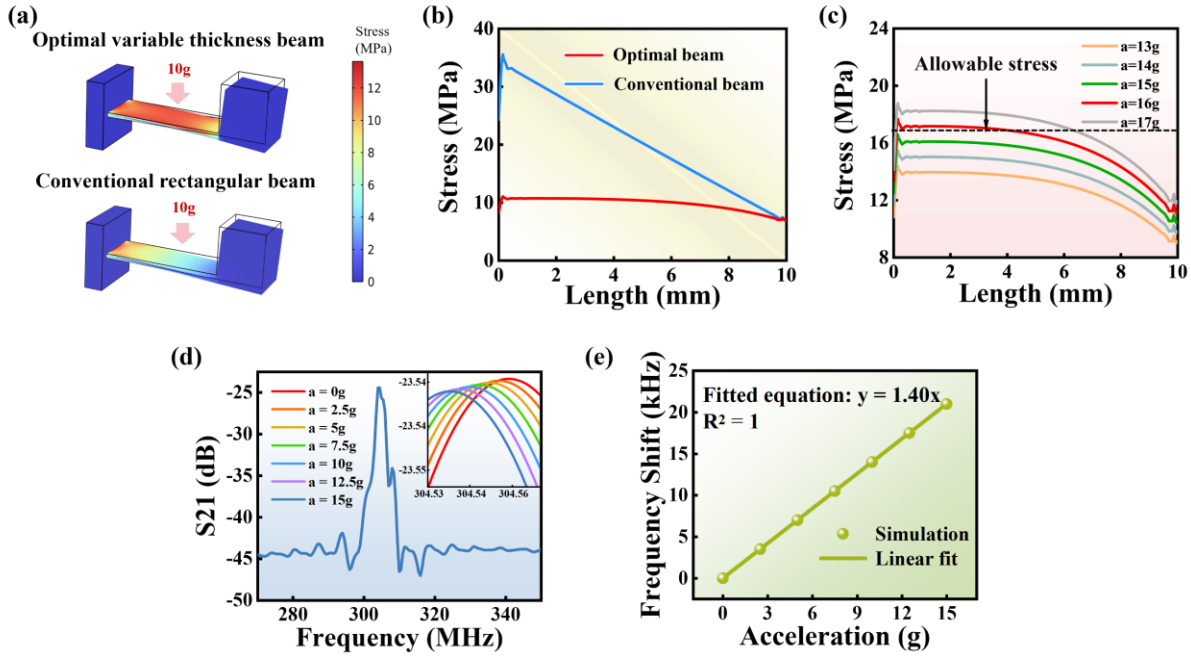

Figure 6. (a) The stress cloud diagram of proposed equal-strength cantilever beam and conventional rectangular cantilever beam under acceleration of 10g; (b) Stress distribution along center line of proposed equal-strength cantilever beam and conventional rectangular cantilever beam; (c) Stress distribution of the cantilever beam under different acceleration loads; (d) The frequency response (transmission coefficient S_{21}) of the SAW accelerometer with a range of 0~15 g; (e) Sensitivity analysis and linear fit of the SAW accelerometer based on equal-strength cantilever.

4.2 SAW Accelerometers Integrated with Equal-strength Beam for High-G

The same analytical process was also carried out for investigating the performance of the accelerometer integrated with proposed simply supported beam. The materials and SAW resonator are the same with these in Section 4.1. The optimization is quite obvious as shown in **Fig. 7a&7b**. The stress on the surface of rectangular simply supported beam changes in a more complicate way, as it firstly increases and then decreases in the area where SAW device is supposed to be mounted. While the stress of the proposed equal-strength simply supported

beam is much more uniform, and provides a wider area suitable for mounting SAW device. Hence, it is also robust to the mounting error of SAW device at the length direction where the SAW device can collect similar strain. Because the middle of the beam is much thicker, which increased the stiffness of the beam, the stress is smaller than that of the conventional model.

Fig. 7c shows that the maximum measurement range is up to 11,500 g, mainly due to the restriction of allowable stress of beam. The frequency responses of such a high-G SAW accelerometer under the large accelerations are calculated (**Fig. 7d**) and the frequency shifts show a good linear relationship versus the varied acceleration, with a linearity coefficient of ~1 and a sensitivity of 6.96 Hz/g (**Fig. 7e**). The sensitivity is much higher than that of previous quartz beam with a sensitivity value of only 0.2 Hz/g[13].

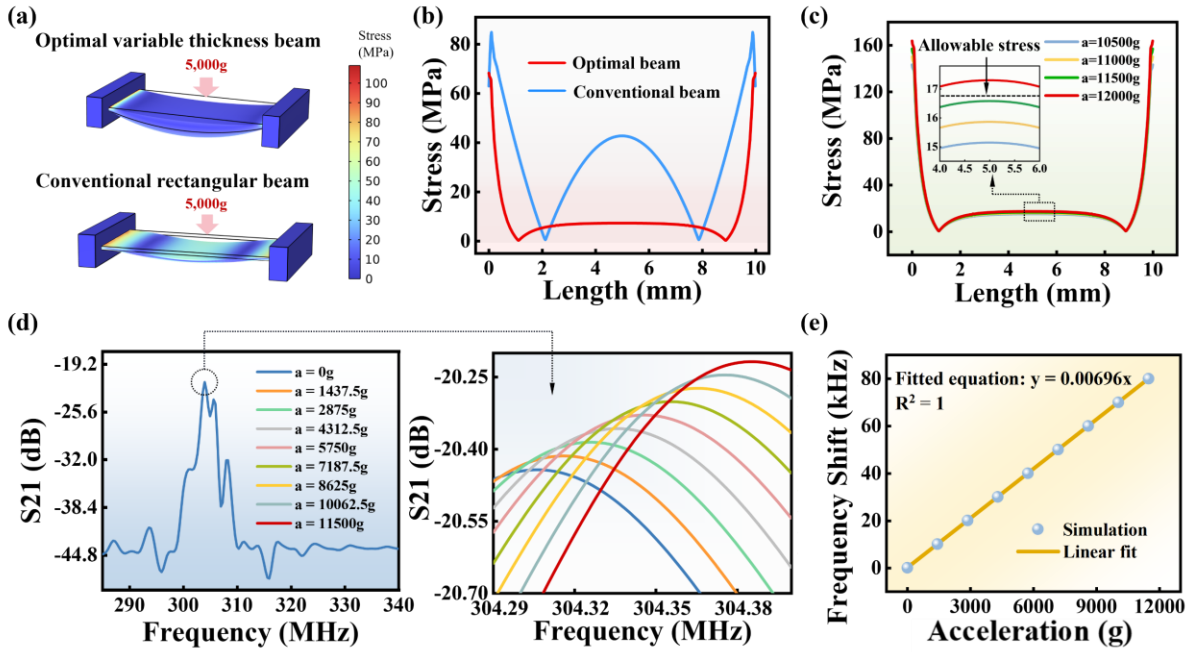

Figure 7. (a) The stress cloud diagram of conventional rectangular simply supported beam and conventional rectangular simply supported beam under acceleration of 5,000g; (b) Stress distribution along center line of proposed equal-strength simply supported beam and conventional rectangular simply supported beam; (c) Stress distribution of the beam under different acceleration loads; (d) The frequency response (transmission coefficient S_{21}) of the SAW accelerometer with a range of 0~11,500 g; (e) Sensitivity analysis and linear fit of the SAW accelerometer based on equal-strength beam;

The characteristics of the SAW accelerometers proposed in this paper are listed in **Table 3** together with those reported in the literature for comparison. We proposed an efficient and accurate simulation platform with coupled the piezoelectric field and mechanics field under the acceleration load, and carried out the analysis of the whole structure of SAW accelerometers, which was never been achieved by the studies in the literature. Furthermore, it is clear that the linearity of our SAW accelerometers with variable thickness equal-strength cantilever beam is still better compared to the rectangular one and triangular one even when the beam length is extremely short. The piezoelectric substrate of SAW device used in this paper is much thicker than the rectangular one, which increases the stiffness of the sensitive structure and leads to attenuation of strain transfer[29]. Hence, the measuring range of our SAW accelerometer with equal-strength cantilever is much larger. In addition, higher sensitivity of SAW accelerometer with variable thickness simply supported beam is achieved.

Table 3. Characteristics of SAW accelerometers

Year	Sensitive Element	Coupled Simulation	Sensitivity	Range	Linearity
2014	Rectangular cantilever beam[11]	No	10.40 kHz/g	0~2.6g	98.1%
2018	Triangular cantilever beam[17]	No	14.25 kHz/g	-1~1g	97.5%
2015	Rectangular simply supported beam[13]	No	0.20 Hz/g	50~65,000g	99.9%
2019	Ring-shaped console[18]	No	0.13 kHz/g	0~8,300g	99.9%
This work	Variable thickness cantilever beam	Yes	1.40 kHz/g	0~15g	99.9%

This work	Variable thickness simply supported beam	Yes	6.96 Hz/g	0~11,500g	99.9%

5. Conclusions

In this paper, a novel simulation platform was developed to analyze and optimize the performance of SAW accelerometer, and a variable-thickness equal-strength cantilever beam was designed to address the issues of non-uniform strain distribution along the cantilever. The proposed simulation platform effectively simulated the frequency responses of SAW devices under the acceleration, visualize the strain/stress distributions, particle displacement field of the sensor, and greatly simplified post-simulation for the related calculations. The accuracy of the model and simulation platform was verified by the experimental result reported by literature. A highly predicted sensitivity equal-strength beam SAW accelerometer was further designed using the simulation platform and its sensitivity was as high as 1.40 kHz/g, a linearity coefficient of ~1 and the measurement range of 0~15 g. Furthermore, a high-G accelerometer was also designed, with the capability of enduring large shocks of up to 11,500 g, and a sensitivity of 6.96 Hz/g. This work lays a foundation for high-performance and robust SAW accelerometers applications.

References

[1] H.E. Ahmed, S. Sahandabadi, Bhawya, M.J. Ahamed, Application of MEMS Accelerometers in Dynamic Vibration Monitoring of a Vehicle, Micromachines 14 (2023). https://doi.org/10.3390/mi14050923

[2] A. Sonnessa, M. Macellari, Dynamic Monitoring of a Railway Steel Bridge with MEMS Accelerometers: First Results on the Case Study of Portella, 22nd International Conference on Computational Science and its Applications (ICCSA), Springer International Publishing Ag, Malaga, SPAIN, 2022, pp. 354-368. https://doi.org/10.1007/978-3-031-10545-6_25

[3] Z.B. Wang, W.Y. Zhou, Z.J. Xiao, Q.R. Yao, X.G. Xia, J. Mei, D. Zhang, P.H. Chen, S.Q. Li, Y.C. Wang, G.H. Rao, S.S. Xie, A High-Temperature Accelerometer with Excellent Performance Based on the Improved Graphene Aerogel, ACS Appl. Mater. Interfaces 15 (2023)

19337-19348. https://doi.org/10.1021/acsami.3c00418

[4] J.J. Geng, L.Y. Xia, J.C. Xia, Q.X. Li, H.Y. Zhu, Y.Z. Cai, Smartphone-Based Pedestrian Dead Reckoning for 3D Indoor Positioning, Sensors 21 (2021) 21. https://doi.org/10.3390/s21248180

[5] C. Wang, F. Chen, Y. Wang, S. Sadeghpour, C. Wang, M. Baijot, R. Esteves, C. Zhao, J. Bai, H. Liu, M. Kraft, Micromachined Accelerometers with Sub-g/Hz Noise Floor: A Review, Sensors (Basel, Switzerland) 20 (2020). https://doi.org/10.3390/s20144054

[6] X.S. Dong, Q.W. Huang, W. Xu, B. Tang, S.H. Yang, J.H. Zhu, Y.F. En, Research on temperature characteristic of parasitic capacitance in MEMS capacitive accelerometer, Sens. Actuator A-Phys. 285 (2019) 581-587. https://doi.org/10.1016/j.sna.2018.12.001

[7] Y.L. Zhao, X.B. Li, J. Liang, Z.D. Jiang, Design, fabrication and experiment of a MEMS piezoresistive high-g accelerometer, Journal of Mechanical Science and Technology 27 (2013) 831-836. https://doi.org/10.1007/s12206-013-0133-8.

[8] Y. Li, L.K. Song, S. Liang, Y.F. Xiao, F.L. Yang, Nonlinear Vibration Study Based on Uncertainty Analysis in MEMS Resonant Accelerometer, Sensors 20 (2020) 19. https://doi.org/10.3390/s20247207.

[9] H.F. Dong, Y.B. Jia, Y.L. Hao, S.M. Shen, A novel out-of-plane MEMS tunneling accelerometer, Sens. Actuator A-Phys. 120 (2005) 360-364. https://doi.org/10.1016/j.sna.2004.12.021

[10] E. Moutoulas, M. Hamidullah, T. Prodromakis, Surface Acoustic Wave Resonators for Wireless Sensor Network Applications in the 433.92 MHz ISM Band, Sensors 20 (2020) 12. https://doi.org/10.3390/s20154294

[11] W. Wang, X.F. Xue, Y.Q. Huang, X.L. Liu, A Novel Wireless and Temperature-Compensated SAW Vibration Sensor, Sensors 14 (2014) 20702-20712. https://doi.org/10.3390/s141120702

[12] W. Wang, Y.Q. Huang, X.L. Liu, Y. Liang, Surface acoustic wave acceleration sensor with high sensitivity incorporating ST-X quartz cantilever beam, Smart Mater. Struct. 24 (2015) 7. https://doi.org/10.1088/0964-1726/24/1/015015

[13] D. Lukyanov, S. Shevchenko, A. Kukaev, M. Khivrich, Ieee, Surface Acoustic Wave Accelerometer for High-G Applications, IEEE International Ultrasonics Symposium (IUS),

Ieee, Taipei, TAIWAN, 2015. https://doi.org/10.1109/ULTSYM.2015.0462

[14] S.Y. Shevchenko, D.A. Mikhailenko, O.A. Markelov, Comparison of AlN vs. SIO2/LiNbO3 Membranes as Sensitive Elements for the SAW-Based Acceleration Measurement: Overcoming the Anisotropy Effects, Sensors 20 (2020) 13. https://doi.org/10.3390/s20020464

[15] S.Y. Shevchenko, D.A. Mikhailenko, Topological Optimization of Circular SAW Resonators: Overcoming the Discreteness Effects, Sensors 22 (2022) 14. https://doi.org/10.3390/s22031172

[16] A.N. Polilov, N.A. Tatus, X. Tian, Analyzing the Correctness of Equal Strength Composite Profiled Beam Bending Problems, J. Appl. Mech. Tech. Phys. 60 (2019) 144-155. https://doi.org/10.1134/S0021894419010188.

[17] S. Shevchenko, A. Kukaev, M. Khivrich, D. Lukyanov, Surface-Acoustic-Wave Sensor Design for Acceleration Measurement, Sensors 18 (2018) 11. https://doi.org/10.3390/s18072301

[18] S.Y. Shevchenko, M.A. Khivrich, O.A. Markelov, Ring-Shaped Sensitive Element Design for Acceleration Measurements: Overcoming the Limitations of Angular-Shaped Sensors, Electronics 8 (2019) 12. https://doi.org/10.3390/electronics8020141

[19] S.V. Biryukov, H. Schmidt, A.V. Sotnikov, M. Weihnacht, T.Y. Chemekova, Y.N. Makarov, Ring waveguide resonator on surface acoustic waves: First experiments, J. Appl. Phys. 106 (2009) 2. https://doi.org/10.1063/1.3272027

[20] D. Lukyanov, S. Shevchenko, A. Kukaev, E. Filippova, D. Safronov, Ieee, Micromechanical Accelerometers Based on Surface Acoustic Waves, 32nd NORCHIP Conference, Ieee, Tampere, FINLAND, 2014. https://doi.org/10.1109/NORCHIP.2014.7004701

[21] Z.B. Ji, J. Zhou, H.M. Lin, J.H. Wu, D.H. Zhang, S. Garner, A. Gu, S.R. Dong, Y.Q. Fu, H.G. Duan, Flexible thin-film acoustic wave devices with off-axis bending characteristics for multisensing applications, Microsyst. Nanoeng. 7 (2021) 9. https://doi.org/10.1038/s41378-021-00325-3

[22] LI Xuan, WANG Wen, HUANG Yangqing, LIU Xinlu, LIANG Yong, The optimization design of surface acoustic wave acceleration sensor with cantilever beam structure, Journal of

Applied Acoustics (2016) 343-350. (in Chinese) https://doi.org/10.11684/j.issn.1000-310X.2016.04.009

[23] Nalamwar, L. A., Surface acoustic waves in strained media, J. Appl. Phys. 47 (1976) 43-48. https://doi.org/10.1063/1.322293.

[24] B.K. Sinha, W.J. Tanski, T. Lukaszek, A. Ballato, Influence of biasing stresses on the propagation of surface waves, J. Appl. Phys. 57 (1985) 767-776. https://doi.org/10.1063/1.334725.

[25] L.J. Kuang, J. Zhou, Y.H. Guo, H.G. Duan, Y.Q. Fu, Versatile and effective design platform for surface acoustic wave accelerometers, Phys. Scr. 98 (2023) 11. https://doi.org/10.1088/1402-4896/ace8cd

[26] F.P. Beer, E. Jr, J.T. Dewolf, D.F. Mazurek, Mechanics of Materials, 7th Edition.

[27] Z.M. Zhou, J.S. Tan, J. Zhang, M. Qin, Structural optimization and analysis of surface acoustic wave biosensor based on numerical method, Int. J. Distrib. Sens. Netw. 15 (2019) 10. https://doi.org/10.1177/1550147719875648

[28] J. R. N. Thurston; H. J. McSkimin; P. Andreatch, Third‐Order Elastic Coefficients of Quartz, J. Appl. Phys. 37 (1966) 267−275. https://doi.org/10.1063/1.1707824

[29] J. Hempel, S. Anees, E. Zukowski, M. Berndt, J. Wilde, L.M. Reindl, Strain Transfer Analysis of Integrated Surface Acoustic Wave Sensors, J. Electron. Packag. 136 (2014) 6. https://doi.org/10.1115/1.4026437